Effect of Orbital Drift and Sensor Changes on the Time Series of AVHRR Vegetation Index Data

Robert K. Kaufmann, Liming Zhou, Yuri Knyazikhin, Nikolay V. Shabanov, Ranga B. Myneni, and Compton J. Tucker

***Abstract*—This paper assesses the effect of changes in solar zenith angle (SZA) and sensor changes on reflectances in channel 1, channel 2, and normalized difference vegetation index (NDVI) from the advanced very high resolution radiometer (AVHRR) Pathfinder land data set for the period July 1981 through September 1994. First, the effect of changes in SZA on channel reflectances and NDVI is derived from equations of radiative transfer in vegetation media. Starting from first principles, it is rigorously shown that the NDVI of a vegetated surface is a function of the maximum positive eigenvalue of the radiative transfer equation within the framework of the theory used and its assumptions. A sensitivity analysis of this relation indicates that NDVI is minimally sensitive to SZA changes, and this sensitivity decreases as leaf area increases. Second, statistical methods are used to analyze the relationship between SZA and channel reflectances or NDVI. It is shown that the use of ordinary least squares can generate spurious regressions because of the nonstationary property of time series. To avoid such a confusion, we use the notion of cointegration to analyze the relation between SZA and AVHRR data. Results are consistent with the conclusion of theoretical analysis from equations of radiative transfer. NDVI is not related to SZA in a statistically significant manner except for biomes with relatively low leaf area. From the theoretical and empirical analysis, we conclude that the NDVI data generated from the AVHRR Pathfinder land data set are not contaminated by trends introduced from changes in solar zenith angle due to orbital decay and changes in satellites (NOAA-7, 9, 11). As such, the NDVI data can be used to analyze interannual variability of global vegetation activity.**

***Index Terms*—AVHRR, interannual variability, NDVI, pathfinder data, satellite drift.**

I. Introduction

A data set of normalized difference vegetation index (NDVI) at 8-km resolution (square pixels) has been produced with data from the advanced very high resolution radiometers (AVHRR) onboard the afternoon-viewing NOAA series satellites (NOAA-7, 9, and 11) under the joint sponsorship of NASA and NOAA Earth Observing System (EOS) Pathfinder Project [1]. The data processing includes improved navigation, intersatellite calibration, and partial correction for Rayleigh scattering. The data are currently available for the period July 1981 to September 1994 and have been used to study interannual variations in global vegetation dynamics. Analysis of the Pathfinder NDVI data indicates increased photosynthetic activity of terrestrial vegetation from 1981 to 1991 in a manner suggestive of an increase in plant growth associated with an increase in the duration of the active growing season [2]. The region of greatest increase lies between 45°N and 70°N, where marked warming has occurred in the spring time due to an early disappearance of snow [3]. The satellite data are consistent with an increase in amplitude of the seasonal cycle of atmospheric CO_2 exceeding 20% since the early 1970's and an advance in the timing of the drawdown of CO_2 in spring and early summer of up to seven days [4].

Conclusions about interannual variability and the biotic effect of climate change are based on a critical assumption: that the data collected by AVHRR's are not contaminated by changes in measurement error over time. If measurement error changes over time, the time series collected by the sensor will contain a deterministic or stochastic trend when none may exist. To avoid confusing these trends with trends generated by changes in terrestrial biota, it is important to identify such errors and correct for their effects before analyzing the data. In the case of the Pathfinder data set, both sensor calibration and illumination variations contribute to measurement error change over time, and the effect of changing illumination, however, can mitigate or enhance the artificial trends caused by calibration instability. The calibration issue has been addressed in numerous scientific studies, but the illumination issue has not. The illumination effect is a combination of the effects of absorption and scattering in the atmosphere and surface anisotropy [5]. In general, properties of both surface and atmosphere vary during the year, which makes the problem even more complex [5]. Quantitative characteristics of atmospheric constituents (aerosol and water vapor) and of the surface are only now becoming available on a global scale. As discussed by Privette *et al.* [6], changes in SZA can affect reflectances by modifying the radiation interactions in the media. Changes in the optical depth of aerosol particles in the troposphere and stratosphere (AOD) affect reflectances directly by changing the reflectivity of the atmosphere [7].

In this paper, we assess the effect of changes in solar zenith angle on reflectances in channel 1, channel 2, and NDVI from the AVHRR Pathfinder land data set assembled from NOAA-7, 9, and 11 sensors (the effect of stratospheric aerosol optical depth is explored in a separate paper). Our assumptions are the following.

1) Most of the artificial signals caused by calibration residuals have been removed by the calibration methods used to process this dataset.

Manuscript received July 27, 1999; revised March 16, 2000. This work was supported by NOAA grant NA76G90481 and NASA Earth Science Enterprise.

R. K. Kaufmann, L. Zhou, Y. Knyazikhin, N. V. Shabanov, and R. B. Myneni are with the Department of Geography, Boston University, Boston, MA 02215 USA (e-mail: kaufmann@bu.edu).

C. J. Tucker is with the Biospheric Sciences Branch, Code 923, NASA Goddard Space Flight Center, Greenbelt, MD 20771 USA.

Publisher Item Identifier S 0196-2892(00)07154-0.

2) Major AOD variations due to volcanic eruptions only cause significant measurement errors within two relatively short periods compared with our whole study period.
3) Residual atmospheric effects were minimized by analyzing the maximum NDVI values within a ten-day interval.

Based on such assumptions, the major signals of changes in reflectances and NDVI are related to changes in SZA, if any. This analysis is described in five sections. In Section II, we derive the effect of changes in SZA on channel reflectances and NDVI from equations of radiative transfer in vegetation media. Starting from first principles, it is rigorously shown that the NDVI of a vegetated surface is a function of the maximum positive eigenvalue of the radiative transfer equation. A sensitivity analysis of this relation is performed to determine the effect of SZA changes on NDVI. It is shown that NDVI is minimally sensitive to SZA changes and that this sensitivity decreases as leaf area increases. The third section describes statistical methods used to analyze the relationship between SZA and channel reflectances or NDVI. It is shown that the use of ordinary least squares (OLS) can generate spurious regressions because the distribution of test statistics in regression models is based on the assumption that time series are stationary, that is, they do not contain a stochastic trend. To avoid confusion about the relation between SZA and NDVI that may be implied by a spurious regression, the notion of cointegration is used to analyze the relation between SZA and AVHRR data. The results of this empirical analysis are described in Section IV, and they are consistent with the conclusion of Section II. NDVI is not related to SZA in a statistically significant manner except for biomes with relatively low leaf area. From the theoretical and empirical analysis, we conclude in Section V that the time series of NDVI generated from the AVHRR Pathfinder land data set are not contaminated by trends introduced from changes in solar zenith angle due to orbital decay and changes in satellites (NOAA-7, 9, 11). As such, the NDVI data can be used to analyze interannual variability of global vegetation activity.

II. Theoretical Analysis

A. Angular Variation of the NDVI

Data for the spectral reflectance recorded by satellite sensors usually are compressed into vegetation indices. The literature describes more than a dozen such indices and these correlate well with vegetation amount [8], the fraction of absorbed photosynthetically active radiation [9], unstressed vegetation conductance and photosynthetic capacity [10], and seasonal atmospheric carbon dioxide variations [11]. These correlations are also supported by theoretical investigations [12]–[15]. This section expands these investigations to analyze the relationship between solar zenith angle (SZA) and NDVI from first principles.

1) Radiative Transfer Problem for Vegetation Media: Consider a vegetation canopy in the layer $0 < z < H$. The top $z = 0$ and bottom $z = H$ surfaces form its upper and lower boundaries. The position vector r denotes the Cartesian triplet (x, y, z) with its origin at the top of the canopy. Assume that photons interact with phytoelements only. That is, photon interactions with optically active elements of the atmosphere inside the layer $0 \leq z \leq H$ are ignored. The radiation field within the layer can be described by the three-dimensional (3-D) transport equation [16], [17]

$$\Omega \cdot \nabla I_\lambda(r,\Omega) + \sigma(r,\Omega) I_\lambda(r,\Omega) = \int_{4\pi} \sigma_{S,\lambda}(r,\Omega' \to \Omega) I_\lambda(r,\Omega')\, d\Omega'. \quad (1)$$

Here, I_λ is the monochromatic radiance which depends on wavelength λ, location r, and direction Ω. The unit vector Ω is expressed in spherical coordinates with respect to $(-Z)$ axis, and $\cos^{-1}\mu$ and ϕ are its polar angle and azimuth. σ is the total interaction cross section, which does not depend on wavelength, and $\sigma_{S,\lambda}$ is the differential scattering cross section. A precise description of these variables can be found in [18], [19]. In the follwing, the formulation of Myneni [19] is adopted.

The transfer equation (1) is a statement of energy conservation in the phase space. The physical meaning of the various terms in (1) is that the first term characterizes the change in radiance in Ω at r, the other terms show whether the changes take place at the expense of absorption and scattering in the medium (second term) and at the expense of the scattering from the other directions (third term).

The magnitude of scattering by elements of the vegetation canopy is described using the hemispherical leaf albedo

$$\omega_\lambda(r,\Omega') = \frac{\int_{4\pi} \sigma_{S,\lambda}(r,\Omega' \to \Omega)\, d\Omega}{\sigma(r,\Omega')}. \quad (2)$$

An individual leaf is assumed to reflect and transmit the intercepted energy in a cosine distribution about the leaf normal. In this case, the leaf albedo ω_λ does not depend on the angular variable (Ω) and the differential scattering cross section $\sigma_{S,\lambda}$ is a symmetrical function with respect to angular variables [20]. It is assumed that the leaf albedo is independent of the spatial variable r. These assumptions are not essential to the following analysis. The typical spectral variation of leaf albedo is defined by three distinct spectral regions [21], i.e., visible (0.4–0.7 μm), near-infrared (0.7–1.35 μm), and mid-infrared (1.35–2.5 μm). In general, a green leaf absorbs 90–95% of solar radiation in the visible region but only 5–10% in the near-infrared. Leaf albedo in the mid-infrared region is usually smaller than in the near-infrared and is controlled by internal leaf structure and absorption by leaf water [22], [23]. Characteristic water absorption bands are at 1.43, 1.95, and 2.2 μm. These properties are inferred from the spectral behavior of a green, healthy leaf and are quite stable although the magnitude of reflectance and transmittance may vary with leaf age and among species. Fig. 1 demonstrates a typical spectral variation of leaf albedo for broadleaf forests. Leaf spectral data were obtained from a variety of sources of filed measurements on different broadleaf trees. The mean and variance spectra were calculated from a large number of samples.

In this study, the normalized differential scattering cross section is used

$$\omega_\lambda g_\lambda(r,\Omega' \to \Omega) = \sigma_{S,\lambda}(r,\Omega' \to \Omega). \quad (3)$$

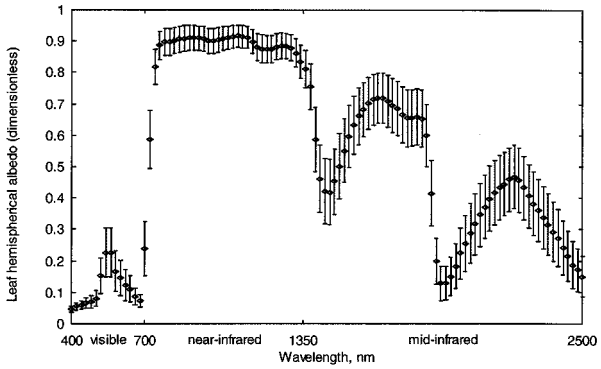

Fig. 1. Mean leaf hemispherical albedo of broadleaf forests and its standard deviation as a function of wavelength.

It follows from (2) that the integral of g_λ over Ω does not depend on the wavelength λ and is equal to total interaction cross section $\sigma(r,\Omega')$, and that the function g_λ is a symmetrical function with respect to angular variables. The coefficient g_λ can be assumed to be independent of wavelength [24]. Substituting (3) in (1) results in

$$\Omega\cdot\nabla I_\lambda(r,\Omega)+\sigma(r,\Omega)I_\lambda(r,\Omega) = \omega_\lambda\int_{4\pi} g(r,\Omega'\to\Omega)I_\lambda(r,\Omega')\,d\Omega'. \tag{4}$$

Let a parallel beam of unit intensity be incident on the upper boundary. At the canopy bottom $z=H$, the fraction of radiation that is reflected back into the canopy by the ground is given by the bidirectional distribution function $\gamma_{b,\lambda}(\Omega',\Omega)$ of the ground. This case is given by the following boundary conditions:

$$I_\lambda(r_0,\Omega)=\delta(\Omega-\Omega_0),\qquad \mu<0 \tag{5}$$

$$I_\lambda(r_H,\Omega)=\pi^{-1}\int_0^{2\pi}d\phi'\int_{-1}^{0}d\mu' \gamma_{b,\lambda}(\Omega',\Omega)|\mu'|I_\lambda(r_H,\Omega'),\qquad \mu>0. \tag{6}$$

Here $\Omega_o\equiv(\mu_o,\phi_o)$ is the direction of the solar parallel beam $\mu_o=\cos(\theta_0),\theta_0$, and ϕ_o are solar polar angle and azimuth angle. δ is the Dirac delta function, and r_0 and r_H denote points on the upper and lower boundaries, respectively. The solution of the boundary value problem, expressed by (4)–(6), describes the radiation field in a vegetation canopy.

The bidirectional reflectance distribution function (BRDF), B_λ, at the spatial point r_0 is defined as the ratio of the mean radiance leaving the top of the plant canopy, $\langle I_\lambda(r_0,\Omega)\rangle_0,\mu>0$, and the incident radiant energy, i.e.,

$$B_\lambda(r_0,\Omega_0,\Omega)=\frac{\langle I_\lambda(r_0,\Omega)\rangle_0}{|\mu_0|}. \tag{7}$$

In the above, the angle bracket $\langle\ \rangle_0$ denotes the mean over the pixel or a horizontal area of interest. $|\mu_0|$ represents the incident radiation energy, because $I_\lambda(r,\Omega)$ in (4) is normalized by the incident radiation. The normalized difference vegetation index (NDVI) is the difference between near-infrared and red BRDF's divided by their sum

$$\mathrm{NDVI}=\frac{B_\beta-B_\alpha}{B_\beta+B_\alpha} \tag{8}$$

where β and α are near-infrared and red spectral wavebands, respectively.

We investigate the relation between solar zenith angle (SZA) changes and NDVI using operator theory [25], [26]. Therefore, we introduce the differential L and integral S operators as

$$LI_\lambda=\Omega\cdot\nabla I_\lambda+\sigma(r,\Omega)I_\lambda(r,\Omega) =\frac{dI_\lambda(r_\gamma+\xi\Omega,\Omega)}{d\xi}+\sigma(r_\gamma+\xi\Omega,\Omega)I_\lambda(r_\gamma+\xi\Omega,\Omega) \tag{9}$$

$$SI_\lambda=\int_{4\pi} g(r,\Omega'\to\Omega)I_\lambda(r,\Omega')\,d\Omega'. \tag{10}$$

In (9), we represent the spatial point r as $r=r_\gamma+\xi\Omega$. Here, the point r_γ belongs to the upper boundary if Ω is directed down (i.e., $\mu<0$) and to the lower boundary otherwise. ξ denotes the distance between the point r and the boundary ($z=0$ or $z=H$) along the direction $-\Omega$. To describe the boundary condition (6), a scattering operator is defined on the lower boundary $z=H$ [27], [28] as

$$R_HI_\lambda(r_H,\Omega)=\pi^{-1}\int_0^{2\pi}d\phi'\int_{-1}^{0}d\mu' \gamma_{b,\lambda}(\Omega',\Omega)|\mu'|I_\lambda(r_H,\Omega'),\qquad \mu>0. \tag{11}$$

Using this notation, the boundary value problem (4)–(6) can be expressed as

$$LI_\lambda=\omega_\lambda SI_\lambda,\quad I_\lambda(r_0,\Omega)=\delta(\Omega-\Omega_0),\quad \mu<0;\qquad I_\lambda(r_H,\Omega)=R_HI_\lambda,\qquad \mu>0. \tag{12}$$

The solution I_λ of (12) is represented by the sum of two components, viz., $I_\lambda=I_{\lambda,0}+\varphi_\lambda$, where $I_{\lambda,0}$ is the incident direct radiation that has not undergone interactions in the canopy, and φ_λ is the intensity of photons scattered one or more times in the canopy (the diffuse component). Because $I_{\lambda,0}=0$ for the upward directions, the diffuse component φ_λ must be specified to evaluate the BRDF (7), i.e.,

$$B_\lambda(r_0,\Omega_0,\Omega)=\frac{\langle\varphi_\lambda(r_0,\Omega)\rangle_0}{|\mu_0|}. \tag{13}$$

Using a standard technique [28], the following boundary value problem for the diffuse component can be derived:

$$L\varphi_\lambda=\omega_\lambda S\varphi_\lambda+\omega_\lambda F,\quad \varphi_\lambda(r_0,\Omega)=0,\qquad \mu<0;\qquad \varphi_\lambda(r_H,\Omega)=R_H\varphi_\lambda+q_\lambda,\qquad \mu>0 \tag{14}$$

where

$$F(r,\Omega)=g(r,\Omega_0\to\Omega)Q(r)\qquad q_\lambda(\Omega)=|\mu_0|\gamma_{b,\lambda}(\Omega_0,\Omega)Q(r_H). \tag{15}$$

The probability density function (Q) that a photon in the beam of direct solar radiation will arrive r along Ω_0 without suffering a collision [19] and [29], can be expressed as

$$Q(r)=\exp\left(-\int_0^{\xi}\sigma(r-\xi'\Omega_0,\Omega_0)\,d\xi'\right). \tag{16}$$

The functions F and q_λ depend on the SZA and determine the effect of changes in SZA on NDVI.

2) Eigenvalues of the Transport Equation: To determine the effect of changes in SZA on NDVI, a sensitivity analysis on the relation between NDVI and the maximum positive eigenvalue of the transport equation is performed. By definition, the eigenvalue of the transport equation is a number γ such that there exists a function φ that satisfies

$$\gamma[\Omega\cdot\nabla\varphi(r,\Omega)+\sigma(r,\Omega)\varphi(r,\Omega)] = \int_{4\pi}\sigma_{s,\lambda}(r,\Omega'\to\Omega)\varphi(r,\Omega')\,d\Omega' \tag{17}$$

with vacuum boundary conditions

$$\varphi(r_0,\Omega)=0\,(\mu<0),\quad \varphi(r_H,\Omega)=0\,(\mu>0). \tag{18}$$

The function $\varphi(r,\Omega)$ is the eigenvector corresponding to the given eigenvalue γ. The set of eigenvalues $\gamma_k, k=0,1,2,\cdots$ and eigenvectors $\varphi_k(r,\Omega), k=0,1,2,\cdots$ of the transport equation is a discrete set [26]. The transport equation has a unique positive eigenvalue that corresponds to a positive eigenvector [26]. This eigenvalue is greater than the absolute magnitudes of the remaining eigenvalues. It provides information intrinsic to the medium (vegetation canopy) and is independent of illumination geometry.

Methods developed in operator theory can be used to estimate the maximum positive eigenvalue. In particular, Krasnoselskii's [30] results on positive operators will be used in the following. Let T be a positive operator, and let u be a positive function for which the following inequality holds:

$$a_1u\le Tu\le b_1u \tag{19}$$

where a_1 and b_1 are some positive constants. Under some general conditions [30], the sequences

$$a_n=\sqrt[n]{\inf\frac{T^nu}{u}},\quad b_n=\sqrt[n]{\sup\frac{T^nu}{u}} \tag{20}$$

converge to the maximum eigenvalue $\eta(T)$ of the operator T from below and above

$$a_n\le\eta(T)\le b_n,\qquad n=1,2,3,\cdots. \tag{21}$$

Knyazikhin [31] discusses conditions under which this result is applicable to the transport equation. The next section shows that the NDVI for a sufficiently dense canopy is a function of the maximum eigenvalue of the operator $T=L^{-1}S$. It follows from (19) and (20) that the maximum positive eigenvalue equation is independent of illumination geometry. Therefore, exploring its relation to NDVI provides the proper analysis to address SZA effects.

B. Dependence of NDVI on SZA in the Case of An Absorbing Ground

Consider the simplest case: reflectance of the ground below the vegetation is zero, that is, $\gamma_{b,\lambda}(\Omega',\Omega)=0$ ($R_H=0, q_\lambda=0$). The problem of radiative transfer in this case is termed the "black soil problem." Results presented in this subsection are required to extend our analysis to the general case of a reflecting soil below the vegetation. We use a standard technique developed in mathematical transport theory [26]–[28] as well as the result mentioned in the previous section.

The solution of the transport equation (14) can be expanded in Neumann series [27], [28] and [32] as

$$\varphi_\lambda=\omega_\lambda f+\omega_\lambda^2Tf+\omega_\lambda^3T^2f+\omega_\lambda^4T^3f+\cdots \tag{22}$$

where $T=L^{-1}S$, $f=L^{-1}F$ are wavelength independent functions. Substituting (22) into (8) and accounting for (13), we obtain

$$\text{NDVI}=\left.\frac{\begin{array}{c}\omega_\beta(1-\theta)f+\omega_\beta^2(1-\theta^2)Tf\\+\omega_\beta^3(1-\theta^3)T^2f+\omega_\beta^4(1-\theta^4)T^3f+\cdots\end{array}}{\begin{array}{c}\omega_\beta(1+\theta)f+\omega_\beta^2(1+\theta^2)Tf\\+\omega_\beta^3(1+\theta^3)T^2f+\omega_\beta^4(1+\theta^4)T^3f+\cdots\end{array}}\right|_{r=r_0}. \tag{23}$$

Here θ is the ratio between leaf albedos at red and near-infrared wavelengths, i.e., $\theta=\omega_\alpha/\omega_\beta$. Note that a typical value of θ varies by about 0.1 (Fig. 1). This allows us to neglect θ^n for $n\ge2$ in (23), which means we neglect the multiple scattering at red spectral band while accounting for multiple scattering radiation at near infrared band. Under these conditions, (23) can be reduced to a rational function whose variation with SZA results from variation of $\omega_\beta(1\pm\theta)f$. Therefore, the following analysis begins with the justification of this technique.

Consider the following functions:

$$\Delta(r,\Omega,\Omega_0,\theta)=\sum_{n=2}^{\infty}\omega_\beta^n\theta^nT^{n-1}f, \tag{24}$$

$$\Phi_0(r,\Omega,\Omega_0)=\sum_{n=2}^{\infty}\omega_\beta^nT^{n-1}f. \tag{25}$$

These expressions can be used to represent NDVI as

$$\text{NDVI}=\frac{\omega_\beta(1-\theta)f+\Phi_0-\Delta}{\omega_\beta(1+\theta)f+\Phi_0+\Delta}. \tag{26}$$

Neglecting the term Δ in (26), the following approximation for NDVI results:

$$\text{NDVI}_0=\frac{\omega_\beta(1-\theta)f+\Phi_0}{\omega_\beta(1+\theta)f+\Phi_0}. \tag{27}$$

The accuracy of this approximation (27) can be investigated by the difference δNDVI = NDVI_0 - NDVI. Because $\varphi_\beta=\omega_\beta f+\Phi_0$

$$\begin{aligned}\delta\text{NDVI}&=2\Delta\frac{\varphi_\beta}{(\varphi_\beta+\omega_\beta\theta f)(\varphi_\beta+\omega_\beta\theta f+\Delta)}\\&\le2\Delta\frac{\varphi_\beta}{(\varphi_\beta+\omega_\beta\theta f)^2}=2\frac{\Delta}{\varphi_\beta}\,\frac{1}{\left(1+\theta\dfrac{\omega_\beta f}{\varphi_\beta}\right)^2}.\end{aligned} \tag{28}$$

Thus, the accuracy of the approximation (27) is proportional to Δ/φ_β.

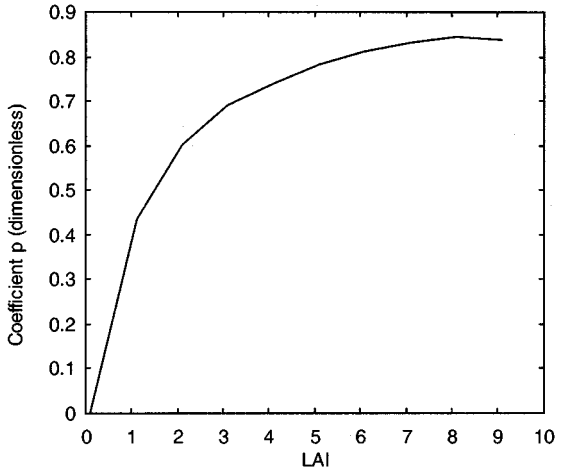

Fig. 2. Coefficient p, which characterizes canopy structure as a function of leaf area index (LAI).

The operator $T = L^{-1}S$ is positive [31]. The positivity of the operator T and equation $\varphi_\beta = \omega_\beta T\varphi_\beta + \omega_\beta f$ imply the following inequalities:

$$\omega_\beta f \le \varphi_\beta, \quad \omega_\beta T\varphi_\beta \le \kappa_\beta \varphi_\beta \tag{29}$$

where

$$\kappa_\beta = \sup_{r,\Omega} \frac{\omega_\beta T\varphi_\beta}{\varphi_\beta} = \sup_{r,\Omega} \left(1 - \frac{\omega_\beta f}{\varphi_\beta}\right) \le 1. \tag{30}$$

The supremum in (30) is taken over all r and Ω, for which $\varphi_\beta(r,\Omega) \neq 0$. This involves the validity of the following transformations:

$$\begin{aligned}\omega_\beta(\omega_\beta T)^n f &\le (\omega_\beta T)^n \varphi_\beta \le (\omega_\beta T)^{n-1}(\omega_\beta T\varphi_\beta) \\ &\le \kappa_\beta(\omega_\beta T)^{n-1}\varphi_\beta \le \cdots \le \kappa_\beta^n \varphi_\beta.\end{aligned} \tag{31}$$

These inequalities allow estimation of the function Δ as

$$\begin{aligned}\Delta(r,\Omega,\Omega_0,\theta) &= \sum_{n=2}^{\infty} \theta^n \omega_\beta(\omega_\beta T)^{n-1} f \\ &\le \sum_{n=2}^{\infty} \theta^n \kappa_\beta^{n-1}\varphi_\beta = \frac{\theta^2\kappa_\beta}{1-\theta\kappa_\beta}\varphi_\beta.\end{aligned} \tag{32}$$

Substituting this inequality in (28) and accounting for the inequality $\omega_\beta f/\varphi_\beta = 1 - \omega_\beta T\varphi_\beta/\varphi_\beta \ge 1 - \kappa_\beta$, one obtains

$$\delta\text{NDVI} \le 2\frac{\theta^2\kappa_\beta}{1-\theta\kappa_\beta} \frac{1}{[1+\theta(1-\kappa_\beta)]^2}. \tag{33}$$

It follows from (19) and (20) that the coefficient κ_β is an estimate of the maximal positive eigenvalue of the operator $\omega_\beta T$ (spectral radius of the operator $\omega_\beta T$). This spectral radius can be estimated as $\omega_\beta p$ [32]. Here, $p = 1 - \exp(-K)$ where K is a wavelength independent constant. Thus, p is a coefficient which depends on canopy structure only. Fig. 2 shows the coefficient p as a function of leaf area index (LAI). Fig. 3 demonstrates variation of δNDVI with respect to θ for different values of κ_β.

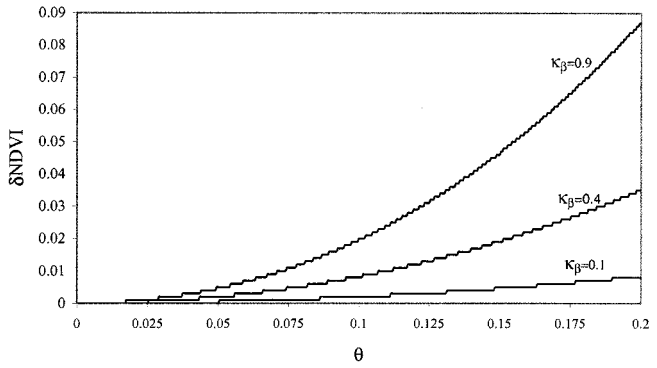

Fig. 3. Difference δNDVI between exactly evaluated NDVI and its approximation as a function of the ratio θ between leaf albedos at red and near-infrared wavelengths for $\kappa_\beta = 0.1$, 0.4, and 0.9.

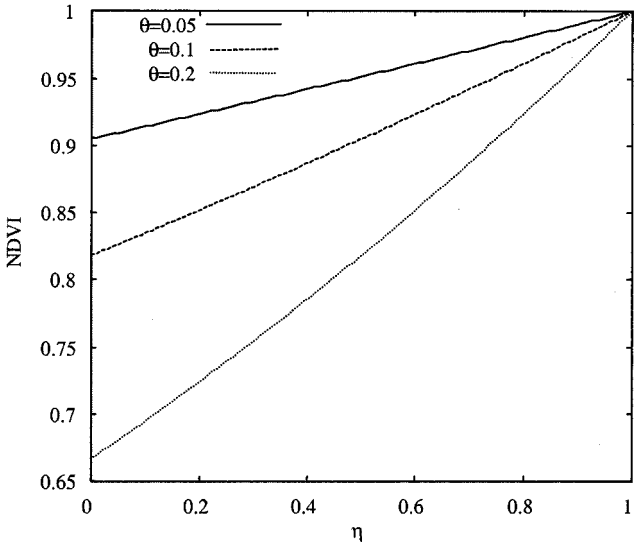

Fig. 4. Range of variation in NDVI caused by variation in canopy structure and sun-view geometry for different values of the ratio θ between leaf albedos at red and near-infrared spectral bands.

δNDVI is less than 0.02 at the typical value of θ (about 0.1) even at the largest $\kappa_\beta = 0.9$. Compared with the range of NDVI values in Fig. 4, one can see that (27) approximates NDVI accurately. Therefore, (27) is used to evaluate NDVI.

Thus, variations in the NDVI are caused by variation in the function f, which is the radiance of photons scattered once. Therefore, the range of variation in NDVI depends on the proportions of Φ_0 and f. To estimate this range, the following function is introduced:

$$\eta(r,\Omega,\Omega_0) = \frac{\omega_\beta T\varphi_\beta}{\varphi_\beta}. \tag{34}$$

It follows from (22), (25), and (34) that $\Phi_0 = \omega_\beta T\varphi_\beta = \eta\varphi_\beta$. The equation $1 = \omega_\beta T\varphi_\beta/\varphi_\beta + \omega_\beta f/\varphi_\beta$ allows $\omega_\beta f$ to be expressed as $\omega_\beta f = (1-\eta)\varphi_\beta$. Substituting Φ_0 and $\omega_\beta f$ in (27), we obtain

$$\text{NDVI}_0 = \frac{(1-\theta)(1-\eta)+\eta}{(1+\theta)(1-\eta)+\eta}. \tag{35}$$

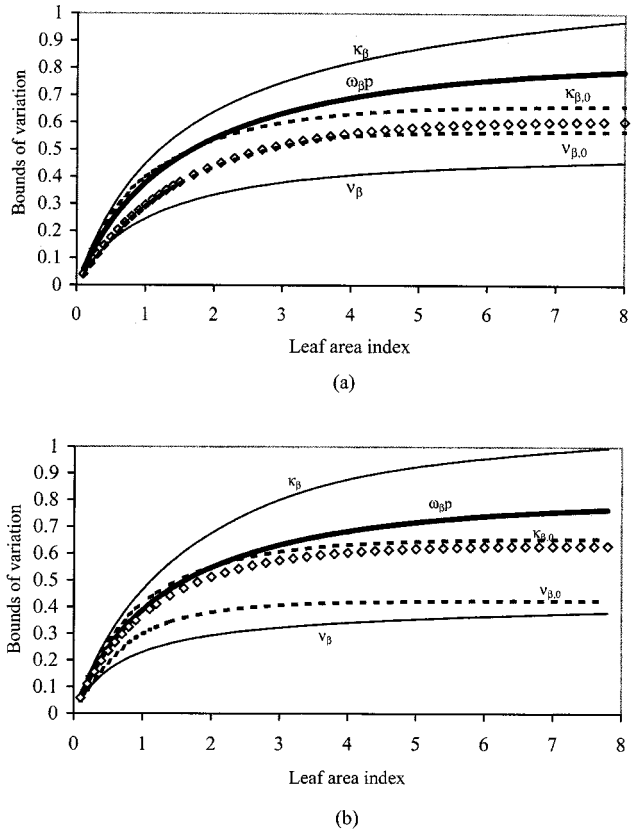

Fig. 5. Upper and lower bounds of variations of $\eta(r,\Omega)$ as a function of LAI for different values of (a) SZA = 15 and (b) SZA = 60. Here, κ_β and ν_β are maximum and minimum of $\eta(r,\Omega)$, taken over all possible spatial points r and directions Ω. $\kappa_{\beta,0}$ and $\nu_{\beta,0}$ are maximum and minimum of $\eta(r,\Omega)$ over points r on the upper canopy boundary and upward directions Ω. $\omega_\beta p$ is the maximum positive eigenvalue (spectral radius) of the transport equation. Values of $\eta(r,\Omega)$ at the upper canopy boundary and in the zenith view direction are depicted with $\diamondsuit$.

It follows from (30) that $0 \le \nu_\beta \le \eta \le \kappa_\beta \le 1$. That is, the range of all possible variations in η does not exceed the interval [0, 1]. Here

$$\nu_\beta = \inf_{r,\Omega} \eta(r,\Omega,\Omega_0) \tag{36}$$

where infinum is taken over all r and Ω, for which $\varphi_\beta(r,\Omega) \neq 0$. The relation between NDVI and η for different values of θ, shown in Fig. 4, indicates that the range of variation in the NDVI is determined by θ, which varies about 0.1 (see Fig. 1) and η. Note that variations in η result from variations in sun-view geometry and canopy structure. From (35), it follows that NDVI can never be less than $(1-\theta)/(1+\theta)$ in the case of a completely absorbing soil. The condition NDVI $\le (1-\theta)/(1+\theta)$ indicates that the case when the ground below the vegetation contributes to the canopy leaving radiation.

Fig. 5 demonstrates the range $[\nu_\beta, \kappa_\beta]$ of variation of η as a function of LAI for different values of the SZA. It follows from (30) and (36) that the upper κ_β and lower ν_β bounds result from variation in r and Ω; that is, at any spatial point r in the canopy and in any direction Ω the values of $\eta(r,\Omega)$ will never be out of the range $[\nu_\beta, \kappa_\beta]$. This interval estimates the spectral radius of the operator $\omega_\beta T$ from above and from below [31], [33], [47], that is, η varies about the spectral radius $\omega_\beta p$. If one constrains variations of r and Ω by spatial points on the upper boundary and view directions (that determines measured NDVI values), the range $[\nu_{\beta,0}, \kappa_{\beta,0}]$ of variation of η becomes essentially narrower. Here, $\kappa_{\beta,0}$ and $\nu_{\beta,0}$ are determined by (30) and (36), respectively, in which supremum and infinum are taken over all r on the upper canopy boundary and view directions. Fig. 5 also shows the upper ($\kappa_{\beta,0}$) and lower ($\nu_{\beta,0}$) bounds as a function of LAI for different values of SZA. The upper bound $\kappa_{\beta,0}$ varies about the spectral radius $\omega_\beta p$, being only slightly sensitive to SZA. The sensitivity of the lower boundary $\nu_{\beta,0}$ to SZA is more discernable. However, this does not result in significant variation in NDVI. For example, the maximum range [$\nu_{\beta,0} = 0.4$, $\kappa_{\beta,0} = 0.65$] of possible variation in η, which corresponds to the low sun position (SZA = 60°) causes NDVI values to vary in the interval [0.88, 0.93] if $\theta = 0.1$, and in [0.78, 0.86] if $\theta = 0.2$ (Fig. 4). It should also be noted that values of η for the zenith view direction are close to the upper bound $\kappa_{\beta,0}$. Thus, in the case of a vegetation canopy with a dark background, variations in NDVI are caused mainly by θ, which describes the optical properties of an individual leaf, and by the parameter p, which describes canopy structure. Both parameters are independent of SZA and view angle. Therefore, we conclude that changes in SZA have no appreciable effect on NDVI.

C. NDVI Variations in the Case of a Reflective Ground

To parameterize the contribution of the surface underneath the canopy (soil and/or understory) to the canopy radiation regime, an effective ground reflectance is introduced, namely [15]

$$\rho_{\text{eff}} = \frac{1}{\pi} \frac{\displaystyle\int_{2\pi-}\int_{2\pi+} \gamma_{b,\lambda}(\Omega',\Omega)|\mu\cdot\mu'|I_\lambda(r_H,\Omega')\,d\Omega\,d\Omega'}{\displaystyle\int_{2\pi-} \mathrm{w}(\Omega')|\mu'|I_\lambda(r_H,\Omega')\,d\Omega'}. \tag{37}$$

The function w is a wavelength-independent configurable function that will be specified later in this section. Note that the effective ground reflectance depends on the solution of the boundary value problem (4)–(6). However, it follows from the definition that the variation of ρ_{eff} satisfies the following inequality:

$$\min_{\Omega'\in 2\pi-} \frac{1}{\pi w(\Omega')} \int_{2\pi+} \gamma_{b,\lambda}(\Omega',\Omega)|\mu|\,d\Omega \le \rho_{\text{eff}}(r_b) \le \max_{\Omega'\in 2\pi-} \frac{1}{\pi \mathrm{w}(\Omega')} \int_{2\pi+} \gamma_{b,\lambda}(\Omega',\Omega)|\mu|\,d\Omega. \tag{38}$$

That is, the range of variations depends on the integrated bidirectional factor $\gamma_{b,\lambda}$ of the ground surface only. Therefore, ρ_{eff} can be taken as a parameter that characterizes ground reflectivity.

To account for the anisotropy of the ground surface, an effective ground anisotropy s_λ is used

$$s_\lambda(r_H,\Omega) = \frac{1}{\rho_{\text{eff}}(\lambda)} \frac{1}{\pi} \frac{\displaystyle\int_{2\pi-} \gamma_{b,\lambda}(\Omega',\Omega)|\mu'|I_\lambda(r_H,\Omega')\,d\Omega'}{\displaystyle\int_{2\pi-} \mathrm{w}(\Omega')|\mu'|I_\lambda(r_H,\Omega')\,d\Omega'},\ \mu > 0. \tag{39}$$

Consider the case when the bidirectional distribution function can be factorized as $\gamma_{b,\lambda}(\Omega',\Omega)=\gamma_{1,\lambda}(\Omega')\gamma_{2,\lambda}(\Omega,\Omega_0)$. Taking

$$\mathrm{w}(\Omega')=\frac{\gamma_{1,\lambda}(\Omega')}{\rho_{1,\lambda}},\quad \rho_{1,\lambda}=\frac{1}{\pi}\int_{2\pi-}\gamma_{1,\lambda}(\Omega')|\mu'|\,d\Omega',$$
$$\rho_{2,\lambda}(\Omega_0)=\frac{1}{\pi}\int_{2\pi-}\gamma_{2,\lambda}(\Omega,\Omega_0)|\mu|\,d\Omega \tag{40}$$

the following expressions for the effective ground reflectance and anisotropy result:

$$\rho_{\mathrm{eff}}=\rho_{1,\lambda}\rho_{2,\lambda}(\Omega_0),\, s_\lambda(r_H,\Omega,\Omega_0)=\frac{\gamma_{2,\lambda}(\Omega,\Omega_0)}{\pi\rho_{2,\lambda}(\Omega_0)}. \tag{41}$$

The integral of $|\mu|s_\lambda(r_H,\Omega,\Omega_0)$ over $\Omega=1$. One can see that the effective ground reflectance and anisotropy do not depend on the solution of the boundary value problem (4)–(6), which can be expressed as [15]

$$\varphi_\lambda(r,\Omega)=\varphi_{BS,\lambda}(r,\Omega)+t_{BS,\lambda}\frac{\rho_{\mathrm{eff}}(\lambda)}{1-\rho_{\mathrm{eff}}(\lambda)j_{s,\lambda}}J_\lambda(r,\Omega). \tag{42}$$

Here, $\varphi_{BS,\lambda}$ is the solution of the black soil problem discussed in the previous section. $t_{BS,\lambda}$ is the downwelling flux at the canopy bottom for the case of the black surface. J_λ and $j_{s,\lambda}$ are radiance and downward flux at the surface level, respectively, generated by the anisotropic source (39) located at the canopy bottom. The function J_λ satisfies the equation $J_\lambda=\omega_\lambda TJ_\lambda+J_s$. Here, J_s is the radiance generated by photons in the anisotropic source (39) located at the canopy bottom that have not undergone any interactions in the canopy. It satisfies the equation $LJ_s=0$ and the boundary condition $J_s(r_0,\Omega)=0$ ($\mu<0$); $J_s(r_H,\Omega)=s_\lambda(r_H,\Omega)$ ($\mu>0$).

Equation (42) includes two extreme situations. The first is the case of a dense canopy, which transmits a negligible amount of radiation, i.e., $t_{BS,\lambda}\approx 0$. The NDVI is evaluated by (35) and is minimally sensitive to variations in the SZA. This is also the case when the surface underneath the canopy is sufficiently dark, i.e., $\rho_{\mathrm{eff}}\approx 0$. Broadleaf forests are an example of such a situation. The second situation is characteristic of a sparse canopy, which transmits almost all incident radiation, i.e., $t_{BS,\lambda}\approx 1$, and scattering from green leaves is negligible. That is, $j_{s,\lambda}\approx 0$, $J_\lambda(r,\Omega)=s_\lambda(r_H,\Omega)$. In this case, NDVI can be calculated as

$$\begin{aligned}\mathrm{NDVI}&=\frac{\rho_{\mathrm{eff}}(\beta)s_\beta(r_H,\Omega)-\rho_{\mathrm{eff}}(\alpha)s_\alpha(r_H,\Omega)}{\rho_{\mathrm{eff}}(\beta)s_\beta(r_H,\Omega)+\rho_{\mathrm{eff}}(\alpha)s_\alpha(r_H,\Omega)}\\&=\frac{\gamma_{b,\beta}(\Omega_0,\Omega)-\gamma_{b,\alpha}(\Omega_0\Omega)}{\gamma_{b,\beta}(\Omega_0,\Omega)+\gamma_{b,\alpha}(\Omega_0,\Omega)}\end{aligned} \tag{43}$$

i.e., the effect of changes in the SZA on NDVI is totally determined by the anisotropy of bare soils.

In conclusion, this analysis indicates that NDVI is minimally sensitive to changes in SZA when the vegetation canopy is sufficiently dense or the surface underneath the canopy is sufficiently dark. This sensitivity is determined by canopy structure only and varies between 1 and $(1-\theta)/(1+\theta)$ (Fig. 4). The sensitivity of NDVI to SZA may increase with decrease in green leaf area of the canopy and/or with increase in ground reflectivity. This process is controlled by the square of canopy transmittance (42), $t_{BS,\lambda}J_\lambda(r_0,\Omega)$. That is, the greater its value, the higher the contribution of the ground to the canopy leaving radiation and, as a consequence, the greater the sensitivity of NDVI to SZA.

III. Empirical Analysis

In this section, the theoretical formulation described above is tested with the NOAA-NASA AVHRR Land Pathfinder data set [1]. First, we describe the preprocessing and compilation of the satellite data. Next, we describe the statistical techniques used to analyze the data.

A. Data Processing

The Pathfinder AVHRR data set includes channel 1 reflectances (red band, 580–680 nm), channel 2 reflectances (near-infrared band, 725–1100 nm), and solar zenith angle from July 1981 to September 1994 at 8 km resolution (square pixels). The data processing included improved navigation, intersatellite calibration, and partial correction for Rayleigh scattering. Correction for atmospheric effects requires information on atmospheric gases, aerosols, clouds, and surface scattering properties. This information is not available, and therefore the NDVI data were composited over a ten-day period. NDVI is calculated from channel 1 and channel 2 reflectances using (8). NDVI is measured on a scale from -1 to 1. For vegetated surfaces, near-infrared reflectance is always greater than red reflectance, therefore NDVI always is positive.

The AVHRR sensor covers the global land surface daily. The quality of these data varies daily due to changes in atmospheric conditions (e.g. clouds and stratospheric aerosols). The daily NDVI data are composited over a ten-day period. Residual atmospheric effects were minimized by analyzing only the maximum NDVI value within each ten-day interval [11] (which generates 474 observations for the sample period). These data generally correspond to observations from near-nadir view direction and clear atmosphere. Compositing the AVHRR data may cause retention of bad scan lines. However, there are very few bad scan lines. Furthermore, spatially averaging on the data, as described below, also helps to reduce the noise caused by these effects.

To reduce the effects of bad scan lines and to compile the data in a way that is consistent with the biophysical parameters by which SZA may affect the AVHRR data (leaf area), we process the Pathfinder AVHRR data (NDVI, Channel 1, Channel 2, and SZA) over the vegetated areas (pixels with positive NDVI) and compile them by biome using a global landcover map [34]. This map identifies 13 biomes (Table I).

The AVHRR data display a significant and relatively constant intrannual seasonality. This pattern is not relevant to the focus of this analysis (the effect of changes in solar zenith angle on interannual variability). Therefore, intrannual variability in the AVHRR and SZA time series is removed as follows. The data are deseasonalized by calculating anomalies from the mean value of the composites for each ten-day compositing period. For example, to calculate NDVI anomalies in the first composited period of August for broadleaf evergreen forests, we calculated the mean NDVI for broadleaf evergreen forests for the

TABLE I
BIOME NO. AND BIOME TYPE OF A GLOBAL LANDCOVER MAP BY DEFRIES *et al.* [34]

Biome No.	Biome Type
1	Evergreen Needleleaf Forests
2	Evergreen Broadleaf Forests
3	Deciduous Needleleaf Forests
4	Deciduous Broadleaf Forests
5	Mixed Forests
6	Woodlands
7	Wooded Grasslands/Shrubs
8	Closed Bushlands or Shrublands
9	Open Shrublands
10	Grasses
11	Croplands
12	Bare
13	Mosses and Lichens
14	All biomes

TABLE II
ORDINARY LEAST SQUARES (OLS) REGRESSION RESULTS FOR (44)–(46)—t TEST $\beta = 0$

Biome	Channel 1	Channel 2	NDVI
1	**8.20**	**8.79**	-1.04
2	**2.46**	**-17.78**	**-2.36**
3	**7.60**	**8.13**	-1.56
4	**9.94**	**5.52**	-1.16
5	**8.19**	**8.72**	-1.05
6	**6.81**	**2.26**	0.66
7	**-2.34**	0.04	**4.41**
8	**-8.92**	**-4.09**	**11.14**
9	**-6.40**	**-2.65**	**12.55**
10	**7.67**	**9.79**	**5.58**
11	**11.89**	**11.89**	-0.19
12	**6.83**	**4.18**	**8.51**
13	**13.19**	**13.50**	-1.66
14	**8.43**	**5.38**	0.77

Values that exceed the 0.05 threshold (|1.96|) are shown in bold

first ten days of August from 1981 through August 1994, subtract this mean from each of the ten-day composited values. Monthly-averaged anomalies are generated from the ten-day composite anomalies (which generates 157 observations for the sample period). Both the ten-day composite and monthly-averaged anomalies are used in the statistical analysis described below.

B. Statistical Methodology

To validate the sensitivity of NDVI to changes in SZA implied by the physics of radiative transfer described in Section II, the AVHRR data anomalies are used to estimate the following models:

$$\text{Channel } 1 = \alpha_1 + \beta_1 * \text{SZA} + \varepsilon_1, \tag{44}$$

$$\text{Channel } 2 = \alpha_2 + \beta_2 * \text{SZA} + \varepsilon_2, \tag{45}$$

$$\text{NDVI} = \alpha_3 + \beta_3 * \text{SZA} + \varepsilon_3 \tag{46}$$

in which Channel 1, Channel 2, and NDVI are derived from the AVHRR Pathfinder data sets [1], SZA is the corresponding solar zenith angle, α and β are regression coefficients, and $\varepsilon_1, \varepsilon_2$, and ε_3 are normally distributed random error terms. These models can be estimated using a variety of statistical techniques, including ordinary least squares (OLS). When using OLS, the effect of changes in solar zenith angle on AVHRR data can be evaluated with a t statistic to test the null hypothesis that $\beta = 0$. Rejecting the null hypothesis would indicate that there is a statistically meaningful relation between solar zenith angle and the AVHRR data. Such a result would indicate that changes in solar zenith angle introduce a trend into the AVHRR data.

We use OLS to estimate (44)–(46) to evaluate the relation between SZA and the ten-day composite AVHRR data described in the previous subsection. Estimating the relation between SZA and channel 1 reflectance (model 1), SZA and channel 2 reflectance (model 2) from this data set indicates that we reject the null hypothesis that $\beta = 0$ for nearly every biome (Table II). These results imply that the data for channel 1 and channel 2 reflectances are influenced by changes in SZA. There is less evidence for a relation between SZA and NDVI (model 3). We cannot reject the null hypothesis that $\beta = 0$ for about half of the biomes (Table II). These results imply that there may be a relation between SZA and NDVI.

Using OLS to estimate (44)–(46) is appealing because of its simplicity. But using OLS to estimate relations between time series carries a significant danger. The distribution of test statistics generated by OLS is based on the assumption that the data are stationary. That is, they do not contain a stochastic trend. If the independent and/or dependent variables in an OLS regression contain a stochastic trend, the regression residual (ε) often will contain a stochastic trend. This violates the assumptions that underline OLS. Such a regression is known as a spurious regression [35]. When evaluated against standard distributions, the correlation coefficients and t statistics for a spurious regression are likely to show that there is a significant relation between the variables when in fact none exists. The possibility for a spurious regression clouds the interpretation of results generated by OLS.

To avoid spurious regressions, we use the notion of cointegration to analyze the relation between solar zenith angle and the AVHRR data. If the data for solar zenith angle contain a stochastic trend, and if this trend "contaminates" channel 1 reflectances, channel 2 reflectances, or NDVI, then SZA will cointegrate with the AVHRR data if the AVHRR data do not contain a separate stochastic trend(s) generated by the terrestrial biota. Cointegration implies that there exists a linear combination of the variables that eliminates the stochastic trend in the data [36]. The linear function(s) that eliminates the stochastic trend is termed a cointegrating vector (CV). For variables that cointegrate, standard inference theory can be used for further hypothesis tests using distributions for cointegrating variables.

The methodology used to examine the relation among SZA and the AVHRR data is carried out in two steps. In the first step, we use statistical tests developed by Dickey and Fuller [37] to determine whether the data for solar zenith angle, channel reflectances, and NDVI contain a stochastic trend. In the second step, we use the full information likelihood procedure developed by Johansen [38], [39] to examine the relation between SZA and channel 1 reflectances, SZA and channel 2 reflectances, and SZA and NDVI. We test two aspects of this relation. First, we ask if there a statistically meaningful relation between SZA and

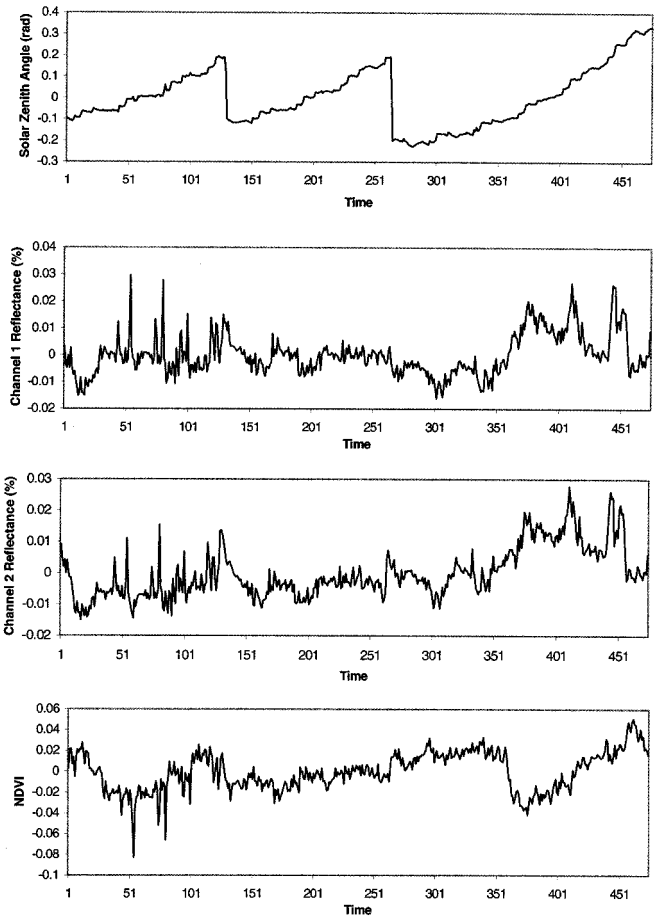

Fig. 6. Globally averaged anomalies of deseasonalized solar zenith angle, channel 1 reflectance, channel 2 reflectance, and NDVI for vegetated areas (where NDVI is positive) from the Pathfinder data set. There are total of 474 samples from July 1981 to September 1994.

the AVHRR data. Second, if there is one present, we ask what is the statistical ordering of this relation (do changes in SZA cause changes in the AVHRR data or vice-versa).

A cursory glance at the time series for SZA indicates that these data are not stationary (Fig. 6). Furthermore, this nonstationarity does not appear to be caused by a deterministic trend. Rather, the data increase fairly steadily over three periods, which are defined by two sharp drops. These drops correspond to changes in satellites (NOAA-7 to NOAA-9, and NOAA-9 to NOAA-11). As such, these changes have a permanent effect on subsequent values for SZA. This persistence implies that the data for SZA contain a stochastic trend.

A stochastic trend is an integrated series of random variables. A random walk in discrete time, which corresponds to Brownian motion in continuous time, is a simple example of a stochastic trend. Stochastic trends are said to be integrated of order one, symbolized as $I(1)$. This terminology indicates that differencing the series once yields a nonintegrated series $I(0)$. An $I(0)$ series is stationary, that is, it does not contain a stochastic or deterministic trend. A deterministic trend is an increase or decrease in a time series that is generated by the passage of time.

We use the augmented Dickey-Fuller (ADF) test [37] to classify the time series for SZA, channel 1 reflectances, channel 2 reflectances, and NDVI as $I(0)$ or I (1). The model for the Dickey-Fuller test is

$$\Delta y_t = \alpha + \beta t + \gamma y_{t-1} \sum_{i=1}^{n} \delta_i \Delta y_{t-1} + \varepsilon_t \qquad (47)$$

where y is the variable under investigation, Δ is the first difference operator, t is a linear time trend (which represents the possible presence of a deterministic trend), α, β, γ, and δ_i are regression coefficients, and ε_t is a random error term. The ADF test evaluates the t-statistic for γ (which is equal to the first order autoregressive coefficient minus one) against a nonstandard distribution. The null hypothesis is that the series is at least $I(1)$. Under this null, $\gamma = 0$. If we can reject this null hypothesis for the undifferenced series, then that series is $I(0)$. If we can only reject the null hypothesis for the differenced series, then that series is $I(1)$. The number of augmenting lagged dependent variables (n) is selected using the Akaike information criterion [40].

TABLE III
VALUES FOR THE DICKEY-FULLER TEST STATISTIC USED TO DETERMINE THE TIME SERIES PROPERTIES OF THE AVHRR AND SZA DATA

Biome	Channel 1	Channel 2	NDVI	SZA
1	**-5.33**	**-4.94**	-3.29	-2.53
2	**-3.49**	-2.99	**-3.80**	-2.80
3	**-5.06**	**-5.01**	**-6.68**	-2.56
4	**-4.00**	**-4.70**	**-3.69**	-2.68
5	**-5.65**	**-5.26**	**-3.74**	-2.39
6	-2.99	**-3.89**	-3.31	-2.98
7	**-3.71**	**-5.67**	-3.06	-2.71
8	**-3.47**	**-5.05**	-2.67	-2.87
9	**-4.45**	**-5.09**	-3.07	-2.69
10	**-5.26**	**-4.42**	-3.18	-2.57
11	**-4.04**	**-4.14**	**-3.94**	-2.58
12	**-5.58**	**-4.65**	**-5.32**	-2.46
13	**-5.17**	**-5.05**	**-4.63**	**-3.61**
14	**-3.60**	**-3.80**	-3.07	-2.82

Values that exceed the 0.05 threshold (-3.42) are shown in bold

The results of the ADF tests for the ten-day data set indicate that the time series properties of SZA, channel 1 reflectances and channel 2 reflectances, and NDVI differ (Table III). The ADF test statistic generated from the levels of SZA fail to reject the null hypothesis (except for biome 13, lichens and mosses), which indicates that the SZA data contain a stochastic trend. Tests on the first difference of the SZA data reject the null hypothesis, which indicate that the SZA data are $I(1)$. The results for the AVHRR data are mixed. The ADF test statistic generated from the levels of channel 1 reflectances reject the null hypothesis (except for biome 6, woodlands), which indicates that these data are $I(0)$. Similarly, the ADF test statistic generated from the levels of channel 2 reflectances reject the null hypothesis (except for biome 2, evergreen broadleaf forests), which indicates that these data are $I(0)$. The ADF test statistic generated from the levels of NDVI are mixed. The test statistic rejects the null hypothesis for seven of the biomes, and fails to reject the null hypothesis for the remaining seven biomes.

The results in Table III undermine conclusions about the relation between SZA and the AVHRR data that are obtained by using OLS. The NDVI data for about half of the biomes have a stochastic trend. For these biomes, it is not possible to determine whether the relation between NDVI and SZA indicated by OLS (Table II) is spurious. For example, OLS indicates that there is a relation between SZA and NDVI in grasslands (biome 10).

But the time series for both SZA and NDVI contain a stochastic trend and therefore, it is not possible to determine whether the relation between these variables for grasslands introduced by OLS is statistically meaningful or is spurious.

For other biomes, the data for SZA contain a stochastic trend while the AVHRR data for NDVI (and channel 1 and channel 2 reflectances) do not. For example, the NDVI time series for biome 7 (wooded grasslands and shrubs) are $I(0)$, while the SZA time series is $I(1)$. These differences are critical because it is not possible for an $I(1)$ variable (SZA) to be related directly to an $I(0)$ variable (most of the channel 1 reflectances, channel 2 reflectances and about half of the NDVI data). Conclusions about the lack of a statistically meaningful relation may be premature because the augmented Dickey-Fuller and other tests for stochastic trends lack power. These tests tend to reject the null too often when the true data generating process is a random walk with noise, and the noise is large compared to the signal [41], [42]. The lower the SNR, the higher the probability of a type I error (i.e., incorrect rejection of the null of a stochastic trend). In a finite sample, reducing the SNR increases the probability that the test will indicate that a variable is trend stationary (that is, a type I error [41]). This conclusion is confirmed by Monte Carlo simulations [43]–[45].

Cursory examination of the data indicate that the signal to noise ratio is low (Fig. 6). Fluctuations in channel 1 reflectances, channel 2 reflectances, and NDVI are large relative to whatever signal may exist. This noise is damped in the monthly-averaged data set (results not shown). Nonetheless, the results of the ADF change only slightly. Reflectances for channel 1 and channel 2 generally are $I(0)$, while the NDVI for about half of the biomes is $I(1)$.

To evaluate whether the AVHRR data cointegrate (share a stochastic trend) with SZA, we use the full information likelihood procedure developed by Johansen [38] and Johansen and Juselius [39] to examine the relation between SZA and channel 1 reflectances, SZA and channel 2 reflectances, and SZA and NDVI. The procedures to estimate cointegrating vectors are derived from a vector autoregression (VAR) in levels, which can be represented as

$$\tilde{y}_t = A_1 y_{t-1} + \cdots + A_k y_{t-k} + \mu + \delta t + \phi\, d_t + \varepsilon_t \quad (48)$$

in which y is a vector of p variables whose behavior is being modeled, k is the number of lags, the A's and ϕ are matrices of regression coefficients, μ and δ are a vector of constants, d_t are nonintegrated exogenous variables, and ε_t is a vector of error terms, each of which is normally independently and identically distributed [46]. $\tilde{y}_t$ is a subset of y, so that (48) can be a part of a larger system of equations.

To test for cointegrating relations among variables in y and to estimate the coefficients of the cointegrating vectors, the VAR is reformulated as a vector error correction model (VECM)

$$\begin{aligned}\Delta\tilde{y}_t =& \Gamma_1 \Delta y_{t-1} + \cdots + \Gamma_{k-1}\Delta y_{t-k+1} \\ &+ \Pi y_{t-1} + \phi \Delta d_t + \mu + \varepsilon_t \end{aligned} \quad (49)$$

where Δ is the first difference operator. Equation (49) specifies the first difference of the $I(1)$ variables, which is stationary, as a function of linear lagged values of the first difference of the nonstationary variables, which also are stationary, and stationary linear combinations of the nonstationary variables, that is, the cointegrating relations.

If there are one or more cointegrating relations, the ECM can be reformulated as follows:

$$\Pi y_{t-1} = \alpha\beta'[1, t, y'_{t-1}] \quad (50)$$

The term $\alpha\beta'\ [1, t, y'_{t-1}]$ indicates that a constant and/or deterministic trend may be included in the cointegrating relation. β' is the matrix of cointegrating vectors, and α is a matrix of coefficients that indicates how each cointegrating relation affects each dependent variable. The significance of coefficients in the (α matrix can be used to infer the statistical ordering in the relation between variables in the cointegrating relation. The number of cointegrating vectors, the variables that make-up a cointegrating vector, the coefficients associated with these variables, and the relation between an ECM and the dependent variables, all can be evaluated using statistics generated by the estimation process.

We specify the VECM (49) to estimate the relation between SZA and channel 1 reflectances (model 1), SZA and channel 2 reflectances (model 2), and SZA and NDVI (model 3). We use no lags ($k = 1$) on the assumption that measurement errors caused by changes in SZA appear in the current measure of channel 1 reflectances, channel 2 reflectances, and NDVI. A VECM is estimated for each of the 13 biomes and global data (biome 14). This implies a total of 42 VECM's.

For each VECM, we determine the number of cointegrating vectors, that is, the number of columns in β' using the λ_{trace} and $\lambda_{\max}$ statistics [38], [39]. The λ_{trace} statistic tests the null hypothesis that the number of cointegrating vectors is less than or equal to r against a general alternative that the number of cointegrating vectors is greater than r. The $\lambda_{\max}$ statistic tests the null hypothesis that the number of cointegrating vectors is r against the specific alternative of r + 1 cointegrating vectors.

The number of cointegrating vectors is used to determine in part the presence of a relation between SZA and channel 1, channel 2, or NDVI. If there is no relation between SZA and the AVHRR data, the λ_{trace} and $\lambda_{\max}$ statistics will not allow us to reject the null hypothesis that there are zero cointegrating vectors. Alternatively, the lack of at least one cointegrating relation could indicate that SZA and the AVHRR data share a stochastic trend, but no cointegrating relation is present because the AVHRR data contain a stochastic trend that originates from the terrestrial biota that is not present in the data for SZA. Rejecting this null hypothesis would indicate that there are one or more cointegrating vectors. This result also signals two possibilities: 1) there are one (or more) linear combinations of SZA and the AVHRR data that are stationary, or 2) the AVHRR and/or SZA data are $I(0)$. The first possibility implies that there is a statistically meaningful relation between SZA and the AVHRR data. The second possibility may imply that there is no relation. By definition, there is one cointegrating vector for each stationary variable in y. So if either the SZA or AVHRR data are $I(0)$, that time series alone could make up a cointegrating relation.

To distinguish between these two possibilities, we use exclusion tests to evaluate restrictions on β that eliminate SZA or the

AVHRR variable from the cointegrating vector. If there is a single cointegrating vector, and the exclusion tests allow us to reject restrictions that eliminate the SZA and the AVHRR variable from the cointegrating relation, both variables are needed to form the cointegrating relation. This result would imply that there is a statistically meaningful (at a specified threshold for statistic significance, $p < 0.05$) relation between SZA and the AVHRR variable. On the other hand, if there is a single cointegrating relation and we cannot reject restriction that eliminates either SZA or the AVHRR variable from the cointegrating relation, this would indicate that the cointegrating relation consists of a single $I(0)$ variable—the variable that cannot be eliminated from the cointegrating relation. In this case, there is no statistically significant relation between SZA and the AVHRR variable.

If there is a relation between SZA and the AVHRR variable, we can determine the statistical ordering of this relation from the statistical significance of the elements of α. The elements of α indicate whether a cointegrating relation affects (loads into) the equation for the first difference of SZA or the AVHRR variable. A statistically significant value for the element of α ($p < 0.05$) indicates that disequilibrium in the long run relation between variables in the cointegrating relation affects the first difference equation. If there is a cointegrating relation between SZA and NDVI, we would expect that the element of α that loads this cointegrating relation into the equation for the first difference of NDVI would be significant. That is, disequilibrium in the long run relation between SZA and NDVI should affect the first difference of the NDVI time series. On the other hand, we would expect that the element of α that loads the cointegrating relation between SZA and NDVI into the first difference of the SZA equation would be insignificant. Disequilibrium in the long run relation between SZA and NDVI should not affect the first difference of the SZA time series.

IV. Results

Conclusions about the number of cointegrating relations in models 1–3 are similar. Both the λ_{trace} and $\lambda_{\max}$ statistics indicate that assigning Π a rank of zero are rejected strongly for all biomes and all models (Table IV). This allows us to reject the possibility that SZA and the AVHRR variable share a stochastic trend, but this cointegration cannot be detected because the AVHRR data also contain a stochastic trend that is introduced by the terrestrial biota (and therefore is not shared by the SZA data). Nearly all models have only one cointegrating relation. Both the λ_{trace} and $\lambda_{\max}$ statistics indicate that assigning Π a rank of 1 cannot be rejected for all models and biomes except biome 13 (mosses and lichens). For this biome, the results of the λ_{trace} and $\lambda_{\max}$ statistics indicate that assigning Π a rank of less than 2 can be rejected. Together, these results imply that the variables in model 1, model 2, and model 3 for biomes other than mosses and lichens contain one cointegrating relation.

Restrictions that eliminate channel 1 reflectances from the single cointegrating relation are rejected strongly in all biomes (Table V). There are ten biomes for which we can reject the restriction that eliminates SZA from the cointegrating relation (Table V). For these ten biomes, there is a statistically meaningful relation between SZA and channel 1 reflectances. This relation is consistent with the analysis in Section II, which indicates that channel 1 reflectances are functions of view and illumination geometry.

TABLE IV
Lambda Statistics for Choosing the Rank of Π

Biome	Ho	Critical Value		Model 1		Model 2		Model 3	
		λmax	λtrace	λmax	λtrace	λmax	λtrace	λmax	λtrace
1	0	14.07	15.41	**40.24**	**40.25**	**34.81**	**34.83**	**57.29**	**57.29**
	1	3.76	3.76	0.02	0.02	0.01	0.01	0.01	0.01
2	0	14.07	15.41	**76.24**	**76.88**	**73.14**	**73.89**	**39.88**	**40.38**
	1	3.76	3.76	0.65	0.65	0.75	0.75	0.50	0.50
3	0	14.07	15.41	**89.65**	**90.84**	**87.92**	**89.17**	**77.77**	**79.04**
	1	3.76	3.76	1.19	1.19	1.25	1.25	1.28	1.28
4	0	14.07	15.41	**76.40**	**76.81**	**56.23**	**56.62**	**50.67**	**51.03**
	1	3.76	3.76	0.41	0.41	0.39	0.39	0.36	0.36
5	0	14.07	15.41	**41.93**	**41.98**	**37.61**	**37.66**	**67.83**	**67.84**
	1	3.76	3.76	0.05	0.05	0.05	0.05	0.01	0.01
6	0	14.07	15.41	**76.45**	**77.78**	**54.58**	**56.00**	**52.47**	**53.65**
	1	3.76	3.76	1.33	1.33	1.42	1.42	1.18	1.18
7	0	14.07	15.41	**108.67**	**109.29**	**73.44**	**74.36**	**42.96**	**43.37**
	1	3.76	3.76	0.62	0.62	0.91	0.91	0.40	0.40
8	0	14.07	15.41	**98.92**	**99.74**	**73.93**	**75.01**	**42.19**	**42.69**
	1	3.76	3.76	0.82	0.82	1.08	1.08	0.51	0.51
9	0	14.07	15.41	**82.65**	**82.94**	**57.08**	**57.45**	**28.78**	**28.88**
	1	3.76	3.76	0.29	0.29	0.37	0.37	0.10	0.10
10	0	14.07	15.41	**40.53**	**40.72**	**33.41**	**33.62**	**29.12**	**29.22**
	1	3.76	3.76	0.20	0.20	0.21	0.21	0.10	0.10
11	0	14.07	15.41	**70.88**	**71.16**	**44.67**	**44.95**	**47.26**	**47.48**
	1	3.76	3.76	0.27	0.27	0.28	0.28	0.22	0.22
12	0	14.07	15.41	**62.06**	**62.17**	**35.19**	**35.28**	**32.93**	**32.93**
	1	3.76	3.76	0.11	0.11	0.09	0.09	0.00	0.00
13	0	14.07	15.41	**56.40**	**62.31**	**53.19**	**58.91**	**58.14**	**63.18**
	1	3.76	3.76	**5.91**	**5.91**	**5.72**	**5.72**	**5.04**	**5.04**
14	0	14.07	15.41	**56.33**	**56.78**	**31.76**	**32.26**	**30.56**	**30.68**
	1	3.76	3.76	0.45	0.45	0.49	0.49	0.30	0.30

Values that exceed the 0.05 threshold (critical values given in the table) are shown in bold.
Ho: Null hypothesis for the number of cointegrating relations.

TABLE V
Tests $\chi^2(1)$ of Exclusion Restrictions on the Cointegrating Relations

Biome	Model 1		Model 2		Model 3	
	Channel 1	SZA	Channel 2	SZA	NDVI	SZA
1	**40.22**	**5.18**	**34.79**	**4.79**	**57.25**	0.00
2	**75.01**	2.58	**71.80**	**25.10**	**39.32**	0.11
3	**87.95**	**6.48**	**86.19**	**7.48**	**76.11**	0.01
4	**75.94**	**15.43**	**55.79**	**4.37**	**50.30**	0.12
5	**41.87**	**5.35**	**37.55**	**5.20**	**67.71**	0.00
6	**74.98**	**8.70**	**52.97**	1.30	**51.27**	0.35
7	**108.01**	1.18	**72.26**	0.22	**42.17**	**8.29**
8	**98.11**	**16.13**	**72.21**	1.78	**41.12**	**18.37**
9	**82.36**	**7.67**	**56.66**	0.51	**27.67**	**13.34**
10	**40.27**	3.77	**33.20**	**5.66**	**28.42**	**5.34**
11	**70.61**	**17.20**	**44.39**	**10.90**	**46.92**	0.11
12	**61.94**	**6.16**	**34.90**	2.52	**32.23**	0.81
13	-	-	-	-	-	-
14	**55.85**	**8.30**	**31.08**	3.19	**30.08**	1.36

Values that exceed the 0.05 threshold (3.89) are shown in bold

For these ten biomes, the nature of the relation between SZA and channel 1 reflectances is indicated by the statistical significance of the elements of α. The statistical significance of the element of α indicates that the cointegrating relations that include SZA and channel 1 reflectances generally load into the equation for the first difference for channel 1 reflectances and generally do not load into the equation for the first difference for SZA (Table VI). This result is consistent with the physical notion that changes in SZA should affect channel 1 reflectances, but changes in channel 1 reflectances do not affect SZA.

The results of model 2 indicate a relation between SZA and channel 2 reflectances, but this relation is present in fewer biomes than the relation between SZA and channel 1 reflectances. For model 2, restrictions that eliminate channel 2 reflectances from the cointegrating relation are rejected strongly in all biomes (Table V). Restrictions that eliminate SZA from

TABLE VI
ELEMENTS OF α USED TO DETERMINE THE STATISTICAL ORDERING OF COINTEGRATING RELATIONS

Biome	Model 1			Model 2			Model 3		
	Channel 1	SZA	Order	Channel 2	SZA	Order	NDVI	SZA	Order
1	**-0.003 (6.392)**	-0.001 (1.726)	SZA→ CH1	**-0.003 (5.999)**	-0.001 (1.007)	SZA→ CH2	**-0.007 (7.587)**	**0.001 (2.345)**	-
2	**-0.003 (9.082)**	-0.001 (0.847)	-	**-0.002 (8.422)**	-0.002 (1.405)	SZA→ CH2	**-0.007 (6.425)**	-0.000 (0.273)	-
3	**-0.018 (9.935)**	**-0.001 (2.937)**	SZA↔ CH1	**-0.017 (9.822)**	**-0.001 (2.447)**	SZA↔ Ch2	**-0.011 (9.141)**	**0.001 (2.600)**	-
4	**-0.003 (9.104)**	-0.001 (0.905)	SZA→ CH1	**-0.002 (7.723)**	-0.000 (0.489)	SZA→ CH2	**-0.005 (7.312)**	0.001 (0.706)	-
5	**-0.004 (6.538)**	-0.001 (1.721)	SZA→ CH1	**-0.003 (6.239)**	-0.001 (1.143)	SZA→ CH2	**-0.007 (8.299)**	**0.002 (3.328)**	-
6	**-0.003 (9.109)**	-0.001 (1.249)	SZA→ CH1	**-0.002 (7.558)**	-0.001 (1.344)	-	**-0.005 (7.414)**	0.000 (0.029)	-
7	**-0.002 (10.886)**	**-0.003 (2.774)**	-	**-0.002 (8.472)**	**-0.003 (3.084)**	-	**-0.004 (6.706)**	0.001 (0.628)	SZA→ NDVI
8	**-0.003 (10.256)**	**-0.003 (2.999)**	SZA↔ CH1	**-0.002 (8.580)**	**-0.003 (2.719)**	-	**-0.003 (6.615)**	0.002 (1.431)	SZA→ NDVI
9	**-0.002 (9.369)**	**-0.002 (2.021)**	SZA↔ CH1	**-0.002 (7.627)**	-0.001 (1.539)	-	**-0.001 (5.411)**	0.001 (1.334)	SZA→ NDVI
10	**-0.002 (6.495)**	-0.00 (0.284)	-	**-0.002 (5.865)**	0.000 (0.064)	SZA→ CH2	**-0.002 (5.458)**	0.001 (0.985)	SZA→ NDVI
11	**-0.003 (8.722)**	-0.001 (1.506)	SZA→ CH1	**-0.002 (6.844)**	-0.001 (0.713)	SZA→ CH2	**-0.004 (7.022)**	0.001 (1.120)	-
12	**-0.002 (8.089)**	-0.001 (1.160)	SZA→ CH1	**-0.001 (6.004)**	0.000 (0.328)	-	**-0.001 (5.839)**	0.002 (1.812)	-
13	-	-	-	-	-	-	-	-	-
14	**-0.002 (7.701)**	-0.001 (1.736)	SZA→ CH1	**-0.001 (5.668)**	-0.001 (0.893)	-	**-0.002 (5.6)**	.001 (1.0)	-

Values that exceed the 0.05 threshold (|1.96|) are shown in bold, and t statistic in parenthesis

the cointegrating relation are rejected in seven biomes. For these seven biomes, there is a statistically meaningful relation between SZA and channel 2 reflectances. Again, this relation is consistent with the analysis in Section II, which indicates that channel 2 reflectances are functions of view and illumination geometry. Consistent with this result, the statistical significance of the elements of α indicate that changes in SZA affect channel 2 reflectances, but changes in channel 2 reflectances generally do not affect SZA (Table VI).

The results for model 3 indicate that the relation between SZA and NDVI is less prevalent than the relation between SZA and the channel reflectances. Exclusion tests indicate that we can reject the restriction that eliminates NDVI from the cointegrating relation for each of the individual biomes and the global data. Tests indicate that we can reject restrictions that eliminate SZA from only four of the individual biomes. For the remaining nine biomes and the global data, we cannot reject restrictions that eliminate SZA from the cointegrating relation. Together, these results indicate that there is no statistically meaningful relation between SZA and NDVI for nine of the biomes and the global data. Conversely, there is a statistically meaningful relation between SZA and NDVI for four biomes. The four biomes in which there is a statistically meaningful relation between SZA and NDVI is slightly less than the six biomes indicated by the models estimated using OLS. This implies that the relation between SZA and NDVI indicated by OLS for two biomes, evergreen broadleaf forests and bare ground, is spurious as defined by [35].

The four biomes for which there is a statistically meaningful relation between SZA and NDVI are consistent with the theoretical analysis described in Section II. The cointegration analysis indicates that there is a statistically meaningful relation between SZA and NDVI in wooded grassland/shrub, closed bushlands, open shrublands, and bushes. None of these biomes are present in the northern latitudes to invalidate the result published in Myneni *et al.* [2]. Each of these biomes has a relatively sparse canopy. A sparse canopy is one of the conditions under which the theoretical analysis indicates that there may be a relation between SZA and NDVI. Thus, the empirical analysis supports the potential for a relation between SZA and NDVI in biomes with spares canopies indicated by the analysis of radiative transfer.

The statistical significance of the elements of α is consistent with the causal order between SZA and NDVI implied by theory. For the four biomes in which there is a relation between SZA and NDVI, the elements of α that represent the effects of disequilibrium in the relation between SZA and NDVI on the first difference of NDVI is statistically significant. This indicates that changes in the long run relation between SZA and NDVI affects NDVI. Conversely, the elements of α that represent the effect of this disequilibrium on the first difference of SZA are insignificant. This indicates that changes in SZA 'cause' changes in NDVI, but changes in NDVI do not cause changes in SZA.

We obtain similar results when we analyze the relation between SZA and monthly averaged AVHRR data (results not shown for brevity). The same four biomes have a statistically meaningful relation between SZA and NDVI: wooded grassland/shrub, closed bushlands, open shrublands, and bushes. Similarly, the statistical significance of the elements of α indicate that changes in SZA cause changes in NDVI but changes in NDVI do cause changes in SZA. Together, these results indicate that data frequency do not affect conclusions about the relation between SZA and NDVI.

V. Conclusions

The results of the empirical analysis of the AVHRR data are consistent with the relation between SZA and the AVHRR data indicated by theory. Equations that describe the physics of radiative transfer in a plant canopy imply that SZA will affect channel 1 and channel 2 reflectances measured by the AVHRR. Consistent with this result, using OLS to estimate model 1 and model 2 indicate a strong relation between reflectances and SZA, regardless of frequency and geographic region. These relations are only slightly weaker when the variables in model 1 and model 2 are examined for cointegration using the full information maximum likelihood procedure developed by Johansen [39].

A physical interpretation of our results is that the NDVI differences with changes in SZA are primarily a soil-induced effect since they become greater with lighter colored soils and they are minimal with very dark soils [47]. In case of dense vegetation canopies, which have high NDVI values, the influence of the soil-induced effect is minimal.

Equations that describe the physics of radiative transfer in a plant canopy imply that the relation between SZA and NDVI should be relative weak. The strength depends on the reflecting surface such that the effect of SZA on NDVI will decrease as leaf area in the canopy increases and the ground under the canopy darkens. The empirical analysis indicates that these conditions are satisfied in a limited number of biomes such that there is a statistically meaningful relation between SZA and NDVI in wooded grassland/shrub, closed bushlands, open shrublands, and bushes. In other biomes, there is no statistically meaningful evidence for a relation between SZA and NDVI. For these biomes, our results imply that the data for NDVI are not contaminated by trends introduced by changes in SZA due to orbital drift and changes in satellite. As such, data for NDVI can be used to analyze interannual variability in the productivity of terrestrial ecosystems.

The presence of a cointegrating relation that includes NDVI only seems to contradict arguments [2] regarding changes in peak greenness and the length of the growing season. A cointegrating relation that includes NDVI only implies that these data do not contain a stochastic trend. Without a stochastic trend, there may be no signal for an elongation in the growing season and an increase in peak greenness. But this seeming contradiction can be resolved by looking at the data examined by [2]. They argue for changes during the growing season only, but this analysis looks for a stochastic trend shared by NDVI and SZA during the entire year. As such, this analysis cannot detect a shared stochastic trend that carries over from one growing season to the next. If such changes are real, such innovations may persist by affecting the amount of biomass that is available at the next growing season. The stochastic trend that would result from such a relation could be detected with the estimation techniques used in this analysis, but would require a different specification. This specification is the focus of future efforts.

References

[1] M. E. James and S. N. V. Kalluri, "The pathfinder AVHRR land data set: An improved coarse resolution data set for terrestrial monitoring," *Int. J. Remote Sensing*, vol. 15, pp. 3347–3364, 1994.

[2] R. Myneni, C. D. Keeling, C. J. Tucker, G. Asrar, and R. R. Nemani, "Increased plant growth in the northern high latitudes from 1981 to 1991," *Nature*, vol. 386, pp. 698–702, 1997.

[3] P. Y. Groisman, T. R. Karl, and R. W. Knight, "Changes of snow cover, temperature, and radiative heat balance over the northern hemisphere," *J. Climate*, vol. 7, pp. 1633–1656, 1994.

[4] C. D. Keeling, J. F. S. Chin, and T. P. Whorf, "Increased activity of northern vegetation inferred from atmospheric CO_2 measurements," *Nature*, vol. 3104, pp. 6241–6255, 1996.

[5] G. G. Gutman, "On the use of long-time global data of land reflectances and vegetation indices derived from the advanced very high resolution radiometer," *J. Geophys. Res.*, 1998.

[6] J. L. Privette, C. Fowler, G. A. Wick, D. Baldwin, and W. J. Emery, "Effects of orbital drift on advanced very high resolution radiometer produces: Normalized difference vegetation index and sea surface temperature," *Remote Sens. Environ.*, vol. 53, pp. 164–171, 1995.

[7] E. Vermote, E. L. Saleous, N. Holben, and B. N. Holben, *Advances in the Use of NOAA AVHRR Data for Land Applications*, G. D'Souza, Ed. Brussels, Belgium, 1995, pp. 93–121.

[8] C. J. Tucker, "Red and photographic infrared linear combination for monitoring vegetation," *Remote Sens. Environ.*, vol. 8, pp. 127–150, 1979.

[9] G. Asrar, M. Fuchs, E. T. Kanemasu, and J. L. Hatfield, "Estimating absorbed photosynthetic radiation and leaf area index from spectral reflectance in wheat," *J. Agron.*, vol. 76, pp. 300–306, 1984.

[10] P. J. Sellers, J. A. Berry, G. J. Collatz, C. B. Field, and F. G. Hall, "Canopy reflectance, photosynthesis and transpiration, III, a reanalysis using improved leaf models and a new canopy integration scheme," *Remote Sens. Environ.*, vol. 42, pp. 187–216, 1992.

[11] C. J. Tucker, Y. Fung, C. D. Keeling, and R. H. Gammon, "Relationship between atmospheric CO_2 variations and a satellite-derived vegetation index," *Nature*, vol. 319, pp. 195–199, 1986.

[12] N. N. Vygodskaya and I. I. Gorshkova, *Theory and Experiment in Vegetation Remote Sensing (in Russian, with English abstract)*. St. Petersburg, Russia: Gidrometeoizdat, 1987, p. 248.

[13] R. B. Myneni, F. G. Hall, P. J. Sellers, and A. L. Marshak, "The interpretation of spectral vegetation indexes," *IEEE Trans. Geosci. Remote Sensing*, vol. 33, pp. 481–486, Mar. 1995.

[14] M. M. Verstraete and B. Pinty, "Designing spectral indexes for remote sensing applications," *IEEE Trans. Geosci. Remote Sensing*, vol. 34, pp. 1254–1265, Sept. 1996.

[15] Y. Knyazikhin, J. V. Martonchik, R. B. Myneni, D. J. Diner, and S. W. Running, "Synergistic algorithm for estimating vegetation canopy leaf area index and fraction of absorbed photosynthetically active radiation from MODIS and MISR data," *J. Geophys. Res.*, vol. 103, pp. 32 257–32 275, 1998.

[16] Y. Knyazikhin, J. Kranigk, R. B. Myneni, O. Panfyorov, and G. Gravenhorst, "Influencee of small-scale structure on radiative transfer and photosynthesis in vegetation cover," *J. Geophys. Res.*, vol. 103, pp. 6133–6144, 1998.

[17] N. V. Shabanov, Y. Knyazikhin, F. Baret, and R. B. Myneni, "Stochastic modeling of radiation regime in discontinuous vegetation canopies," *Remote Sens. Environ.*, 2000, to be published.

[18] J. Ross, *The Radiation Regime and Architecture of Plant Stands*, W. Junk, Ed. Norwell, MA, 1981, p. 391.

[19] R. B. Myneni, "Modeling radiative transfer and photosynthesis in three-dimensional vegetion canopies," *Agric. Forestry Meteorol.*, vol. 55, pp. 323–344, 1991.

[20] J. K. Shultis and R. B. Myneni, "Radiative transfer in vegetation canopies with anisotropic scattering," *J. Quant. Spectrosc. Radiat. Transf.*, vol. 39, no. 2, pp. 115–129, 1988.

[21] E. A. Walter-Shea and J. M. Norman, *Leaf Optical Properties, in Photon-Vegetation Interactions: Applications in Plant Physiology and Optical Remote Sensing*, R. B. Myneni and J. Ross, Eds. New York: Springer-Verlag, 1991, pp. 229–251.

[22] E. B. Knipling, "Physical and physiological basis for the reflectanct of visible and near-infrared radiation from vegetation," *Remote Sens. Environ.*, vol. 1, pp. 155–159, 1970.

[23] J. T. Woolley, "Reflectance and transmittance of light by leaves," *Plant Physiol.*, vol. 47, pp. 656–662, 1971.

[24] O. Panferov, Y. Knyazikhin, R. B. Myneni, J. Szarzynski, S. Engwald, K. G. Schnitzler, and G. Gravenhorst, "The role of canopy structure in the spectral variation of transmission and absorption of solar radiation in vegetation canopies," *IEEE Trans. Geosci. Remote Sensing*, to be published.

[25] R. D. Richtmyer, *Principles of Advanced Mathematical Physics*. New York: Springer-Verlag, 1978, p. 422.

[26] V. S. Vladimirov, "Mathematical problems in the one-velocity theory of particle transport," Tech. Rep. AECL-1661, At. Energy Can. Ltd., Chalk River, ON, Canada, 1963.

[27] T. A. Germogenova, *The Local Properties of the Solution of the Transport Equation (in Russian)*. Moscow, Russia: Nauka, 1986, p. 272.

[28] J. Y. Ross, Y. Knyazikhin, A. Kuusk, A. Marshak, and T. Nilson, *Mathematical Modeling of the Solar Radiation Transfer in Plant Canopies (in Russian, with English abstract)*. St. Peterburg, Russia: Gidrometeoizdat, 1992, p. 195.
[29] Y. Knyazikhin, G. Miessen, O. Panfyorov, and G. Gravenhorst, "Small-scale study of three-dimensional distribution of photosynthetically active radiation in a forest," *Agric. Forestry Meteorol.*, vol. 88, pp. 215–239, 1997.
[30] M. A. Krasnoselskii, *Positive Solutions of Operator Equations*. Groningen: P. Noordhof, 1964, p. 378.
[31] Y. V. Knyazikhin, "On the solvability of plane-prallel problems in the theory of radciation transport," *U.S.S.R. Comput. Math. Phys.*, vol. 30, no. 2, pp. 145–154, 1990.
[32] Y. Knyazikhin and A. Marshak, *Fundamental Equations of Radiative Transfer in Leaf Canopies and Iterative Methods for Their Solution in Photon-Vegetation Interactions: Applications in Plant Physiology and Optical Remote Sensing*, R. B. Myneni and J. Ross, Eds. New York: Springer-Verlag, 1991, pp. 9–43.
[33] S. G. Krein, *Functional Analysis*, S. G. Krein, Ed. Moscow, Russia: Naukapp, 1972, p. 544.
[34] R. S. DeFries, M. Hansen, J. Townshend, and R. Sohlberg, "Global land cover classifications at 8 km spatial resolution: The use of training data derived from Landsat imagery in decision tree classifiers," *Int. J. Remote Sensing*, vol. 19, no. 16, pp. 3141–3168, 1998.
[35] C. W. J. Granger and P. Newbold, "Spurious regressions in econometrics," *J. Econometrics*, vol. 35, pp. 143–159, 1974.
[36] R. E. Engle and C. W. J. Granger, "Cointegration and error-correction: Representation, estimation, and testing," *Econometrica*, vol. 55, pp. 251–276, 1987.
[37] D. A. Dickey and W. A. Fuller, "Distribution of the estimators for autoregressive time series with a unit root," *J. Amer. Statist. Assoc.*, vol. 74, pp. 427–431, 1979.
[38] S. Johansen, "Statistical analysis of cointegration vectors," *J. Econ. Dynam. Contr.*, vol. 12, pp. 231–254, 1988.
[39] S. Johansen and K. Juselius, "Maximum likelihood estimation and inference on cointegration with application to the demand for money," *Oxford Bull. Econ. Statist.*, vol. 52, pp. 169–209, 1990.
[40] H. Akaike, "Information theory and an extension of the maximum likelihood principle," in *2nd Int. Symp. Information Theory*, B. N. Petrov and F. Csaki, Eds. Budapest: Akademini Kiado, 1973, pp. 267–281.
[41] W. Enders, *Applied Econometric Time Series*. New York: Wiley, 1995.
[42] J. D. Hamilton, *Time Series Analysis*. Princeton, NJ: Princeton Univ. Press, 1994.
[43] G. W. Schwert, "Tests for unit roots: A Monte Carlo investigation," *J. Bus. Econ. Statist.*, vol. 7, pp. 147–159, 1989.
[44] P. C. B. Phillips and P. Perron, "Testing for a unit root in time series regression," *Biometrika*, vol. 75, pp. 335–346, 1988.
[45] K. Kim and P. Schwert, "Some evidence on the accuracy of the Phillips-Perron tests using alternative estimates of nuisance parameters," *Econ. Lett.*, vol. 34, pp. 345–350, 1990.
[46] H. Hansen and K. Juselius, *CATS in RATS: Cointegration Analysis of Time Series*. Evanston, IL: Estima, 1995.
[47] G. Asrar, *Theory and Applications of Optical Remote Sensing*. New York: Wiley, 1989, ch. 4, pp. 125–125.

Robert K. Kaufmann received the B.S. degree in ecology and systematics from Cornell University, Ithaca, NY, in 1979, the M.A. degree in economics from the University of New Hampshire, Durham, NH, in 1984, and the Ph.D. degree in energy management and policy from the University of Pennsylvania, Philadelphia, in 1988.

Currently, he is an Associate Professor with the Department of Geography and the Center for Energy and Environmental Studies, Boston University, Boston, MA. His research focuses on the attribution of climate change to human activity, the impacts of global climate change, world energy markets, and land use change in the Pearl River Delta in China.

Liming Zhou received the B.S. and M.S. degrees in meteorology from Nanjing Institute of Meteorology, Nanjing, China, in 1991 and 1994, respectively. He is currently pursuing the Ph.D. degree in the Department of Geography, Boston University, Boston, MA, where he is working on the relation between interannual variability in climate change and global vegetation dynamics observed from satellite sensed dataset.

Yuri Knyazikhin received the M.S. degree in applied mathematics from Tartu University, Tartu, Estonia, in 1978, and the Ph.D. degree in numerical analysis from the N.I. Muskhelishvilli Institute of Computing Mathematics, the Georgian Academy of Sciences, Tbilisi, Georgia, in 1985.

From 1978 to 1990, he was a Research Scientist with the Institute of Astrophysics and Atmospheric Physics and the Computer Center of the Siberian Branch of the Russian Academy of Sciences, Tartu University. He was with the University of Göttingen, Göttingen, Germany, from 1990 to 1996. He is currently a Research Associate Professor, Department of Geography, Boston University, Boston, MA. He has worked and published in areas of numerical integral and differential equations, theory of radiation transfer in atmospheres and plant canopies, remote sensing of the atmosphere and plant canopies, ground-based radiation measurements, forest ecosystem dynamics, and modeling sustainable multifunctional forest management.

Dr. Knyazikhin was an Alexander von Humboldt Fellow from 1992 to 1993.

Nikolay V. Shabanov received the M.A degree in physics from Moscow State University, Moscow, Russia, in 1996, and the M.A. degree in geography from Boston University, Boston, MA, in 1999. He is currently pursuing the Ph.D. degree in the Department of Geography, Boston University, Boston, MA, where he is working on the analysis of satellite vegetation index data for ecosystem structure changes.

Ranga B. Myneni received the Ph.D. degree in biology from the University of Antwerp, Antwerp, Belgium, in 1985.

Since 1985, he has been with Kansas State University, Manhattan, the University of Göttingen, Göttingen, Germany, and NASA Goddard Space Flight Center, Greenbelt, MD. He is currently on the Faculty of the Department of Geography, Boston University, Boston, MA. His research interests are in radiative transfer, remote sensing of vegetation, and climate-vegetation dynamics.

Dr. Myneni is a MODIS and MISR science team member.

Compton J. Tucker received the B.S. degree in biology and the M.S. and Ph.D. degrees in forestry from Colorado State University, Fort Collins, in 1969, 1973, and 1975, respectively.

He has been with NASA Goddard Space Flight Center, Greenbelt, MD, for over 20 years, planning and conducting research on deforestation and the Earth's climate and biogeochemical cycles.